

Updated Results of a Solid-State Sensor Irradiation Study for ILC Extreme Forward Calorimetry

Talk presented on behalf of the FCAL Collaboration at the International Workshop on Future Linear Colliders (LCWS2016), Morioka, Japan, 5-9 December 2016. C16-12-05.4.

Paul Anderson, Wyatt Crockett, Luc D'Hauthuille, Vitaliy Fadeyev, Caleb Fink, Cesar Gonzalez Renteria, Benjamin Gruey, Jane Gunnell, Forest Martinez-McKinney, Greg Rischbieter, Kyle Rocha, Bruce A. Schumm*, Edwin Spencer, Max Wilder

Santa Cruz Institute for Particle Physics and the University Of California, 1156 High Street, Santa Cruz, California 95064 USA

Abstract

Detectors proposed for the International Linear Collider (ILC) incorporate a tungsten sampling calorimeter ('Beam-Cal') intended to reconstruct showers of electrons, positrons and photons that emerge from the interaction point of the collider with angles between 5 and 50 milliradians. For the innermost radius of this calorimeter, radiation doses at shower max are expected to reach 100 Mrad per year, primarily due to minimum-ionizing electrons and positrons that arise in the induced electromagnetic showers of e^+e^- 'beamstrahlung' pairs produced in the ILC beam-beam interaction. However, radiation damage to calorimeter sensors may be dominated by hadrons induced by nuclear interactions of shower photons, which are much more likely to contribute to the non-ionizing energy loss that has been observed to damage sensors exposed to hadronic radiation. We report here on prior highlights and recent results of SLAC Experiment T-506, for which several different types of semiconductor sensors were exposed to doses of radiation induced by showering electrons of energy 3.5-13.3 GeV. By embedding the sensor under irradiation within a tungsten radiator, the exposure incorporated hadronic species that would potentially contribute to the degradation of a sensor mounted in a precision sampling calorimeter. Depending on sensor technology, significant post-irradiation charge collection was observed for doses of several hundred Mrad.

Keywords:

Semiconductor sensors, Radiation damage, ILC Beamline Calorimeter

1. Introduction

Far-forward calorimetry, covering the region between 5 and 50 milliradians from the on-energy beam axis, is envisioned as a component of both the ILD [1] and SiD [2] detector concepts for the proposed International

Linear Collider (ILC). The BeamCal tungsten sampling calorimeter proposed to cover this angular region is expected to absorb approximately 10 TeV of electromagnetic radiation per beam crossing from e^+e^- beamstrahlung pairs, leading to expected annual radiation doses of 100 Mrad for the most heavily-irradiated portions of the instrument. While the deposited energy is expected to arise primarily from minimum-ionizing electrons and positrons in the induced electromagnetic

*Corresponding author.

Email address: baschumm@ucsc.edu (Bruce A. Schumm)

showers, radiation damage to calorimeter sensors may be dominated by hadrons induced by nuclear interactions of shower photons, which are much more likely to contribute to the non-ionizing energy loss that has been observed to damage sensors exposed to hadronic radiation. We report here on the latest results of SLAC Experiment T-506, for which several different types of solid-state sensors were exposed to doses of up to 300 Mrad at the approximate maxima of electromagnetic showers induced in a tungsten radiator by electrons of energy 3.5-13.3 GeV, similar to that of electrons and positrons from ILC beamstrahlung pairs.

Bulk damage leading to the suppression of the electron/hole charge-collection efficiency (CCE) is generally thought to be proportional to the non-ionizing energy loss ('NIEL') component of the energy deposited by the incident radiation. Observations from early studies of electromagnetically-induced damage to solar cells [3, 4, 5] suggested that p-type bulk sensors were more tolerant to damage from electromagnetic sources, due to an apparent departure from NIEL scaling, particularly for electromagnetic particles of lower incident energy.

Several more-recent studies have explored radiation tolerance of silicon diode to incident fluxes of electrons. A study assessing the capacitance vs. bias voltage (CV) characteristics of sensors exposed to as much as 1 Grad of incident 2 MeV electrons [6] suggested approximately 35 times less damage to n-type magnetic Czochralski sensors than that expected from NIEL scaling. A study of various n-type sensor types exposed to 900 MeV electrons showed charge-collection loss of as little as 3% for exposures up to 50 Mrad [7]; for exposures of 150 Mrad, the degree of damage was observed to be as small as one-fourth that expected from NIEL scaling [8]. These discrepancies have been attributed to the different types of defects created by lattice interactions: electrons tend to create point-like defects that are more benign than the clusters formed due to hadronic interactions.

Finally, in studies of sensors exposed to large doses of hadron-induced radiation, p-type bulk silicon was found to be more radiation-tolerant than n-type bulk silicon, an observation that has been attributed to the absence of type inversion and the collection of an electron-based signal [9, 10]. However, n-type bulk devices have certain advantages, such as a natural inter-electrode isolation with commonly used passivation materials such as silicon oxide and silicon nitride.

More recently, a number of non-diode solid-state sensors have been proposed as a possible radiation-tolerant alternative to silicon sensors, the latter of which can de-

velop a large dark current after significant irradiation. Here, we report on an exploration of the radiation tolerance of silicon-diode pad sensors and several bulk solid-state pad sensors, including gallium arsenide (GaAs), silicon carbide (SiC) and industrial sapphire sensors. The sensors' radiation tolerance is assessed via direct measurements of the median collected charge deposited by minimum-ionizing particles as well as leakage current measurements. Note that while diode sensors must be operated with the sense of bias voltage that provides a reverse bias, bulk sensors can in principle be operated with either sign of the bias voltage. When results are presented below for bulk sensors with only one sign of the bias voltage, they are presented for the sign that provided the best performance.

Two n-type and one p-type bulk silicon diode sensors were explored. The p-bulk sensor ('WSI-P4' or 'PF'), from a test structure associated with a prototype sensor developed for the ATLAS upgrade tracker [11], was fabricated by the Hamamatsu Photonics Corporation (HPK) from a float-zone crystal with a thickness of 320 μm , and had an un-irradiated depletion voltage of approximately 180 V. The first of the n-bulk sensors ('N6906' or 'NF'), from a test structure associated with sensors developed for the Fermi satellite [12], was also manufactured by HPK from a float zone crystal, in this case with a thickness of 400 μm , and an un-irradiated depletion voltage of less than 40 V. In addition, the radiation tolerance of a 320 μm -thick n-type pad structure designed for use in the ILC Luminosity Calorimeter (LumiCal), which would cover the angular region just outside that of the BeamCal, was explored. The sensor was manufactured by HPK; further details about the sensor design can be found in [13]

This study made use of a fragment of a LumiCal sensor that had been accidentally broken; once the broken sensor was obtained by SCIPP, a study was done to determine, qualitatively, how the leakage current of a given pad depended upon that pad's proximity to the guard ring and the cleaved edge. Based on this understanding, the fragment was intentionally cleaved into two small pieces that could be mounted on the daughter boards used in the radiation target and charge-collection-efficiency apparatus. After a regimen of exposing the sensor to elevated temperature, and exposing the cleaved edge to ultraviolet light, it was found that the sensor could be biased to over 200 V without breaking down (i.e. developing a leakage current greater than several μA), well above the depletion voltage of 40 V. This allowed pre-irradiation charge-collection data to be taken at full depletion. The irradiation process further raised the breakdown voltage, allowing post-irradiation

data to be taken at bias voltages as high as 400 V.

The GaAs sensor used in the study was produced by means of the Liquid Encapsulated Czochralski method doped by a shallow donor (Sn or Te; Sn was used for the sensor in this study) [14], and had a bulk thickness of 300 μm . The SiC sensor used in the study featured double-layer nickel-gold Schottky-barrier contacts mounted on a 4H-SiC crystal structure. The sensors were 420 μm thick, with an high quality epitaxial (active) layer of thickness 70 μm and an inactive substrate thickness of 350 μm . More details about this sensor and its performance can be found in [15]. The industrial sapphire sensor used in the study had a thickness of 520 μm , and was produced by Crystal GmbH, Berlin. A three-layer metal contact consisting of aluminum (at the crystal surface) overlain with platinum and then gold was applied at the GSI laboratory in Darmstadt.

Prior results on the radiation tolerance of the GaAs sensor, as well as of silicon diode sensors, including a p-type float-zone sensor irradiated to a dose of 270 Mrad, are presented in [16] and [17]. New to this report are results for n-type float-zone and sapphire sensors irradiated to 300 Mrad, and for a 77 Mrad irradiation of the SiC sensor. Extended annealing studies are also presented for the GaAs sensor and for the p-type float-zone sensor that was irradiated to 270 Mrad.

While the radiation dose was initiated by electromagnetic processes (electrons showering in tungsten), the placement of the sensors near shower max ensures that the shower incorporates an appropriate component of hadronic irradiation arising from neutron spallation, photoproduction, and the excitation of the Δ resonance. Particularly for the case that NIEL scaling suppresses electromagnetically-induced radiation damage, the small hadronic component of the electromagnetic shower might dominate the rate of damage to the sensor. However, the size and effect of this component is difficult to estimate reliably, and so we choose to study radiation damage in a configuration that naturally incorporates all components present in an electromagnetic shower.

2. Experimental Setup

Un-irradiated sensors were subjected to current vs. bias voltage (IV) and capacitance vs. bias voltage (CV) tests, the results of which allowed a subset of them to be selected for irradiation based on their breakdown voltage (typically above 1000 V for selected sensors) and low level of leakage current. The sensors were placed on carrier printed-circuit ‘daughter boards’

and wire-bonded to a readout connector. The material of the daughter boards was milled away in the region to be irradiated in order to facilitate the charge collection measurement (described below) and minimize radio-activation. The median collected charge was measured with the Santa Cruz Institute for Particle Physics (SCIPP) charge-collection (CC) apparatus (also described below) before irradiation. The sensors remained mounted to their individual daughter boards throughout irradiation and the followup tests, simplifying their handling and reducing uncontrolled annealing. Additionally, this allowed a reverse-bias voltage to be maintained across the sensor during irradiation. This voltage was kept small (at the level of a few volts) to avoid possible damage of the devices from a large instantaneous charge during the spill.

Sensors were irradiated with beam provided by the End Station Test Beam (ESTB) facility at the SLAC National Accelerator Laboratory. Parameters of the beam provided by the ESTB facility are shown in Table 1. The beam was incident upon a series of tungsten radiators. An initial 7mm-thick (2.0 radiation-length) tungsten plate (‘R1’) served to initiate the electromagnetic shower. The small number of radiation lengths of this initial radiator permitted the development of a small amount of divergence of the shower relative to the straight-ahead beam direction without significant development of the largely isotropic hadronic component of the shower.

Table 1: Parameters of the beam delivered by the ESTB facility during the T-506 experiment.

Parameter	Value
Energy	3.5-14.5 GeV
Repetition Rate	5-10 Hz
Charge per Pulse	150-180 pC
Spot Size (radius)	~ 1 mm

This plate was followed by an open length of approximately half a meter, which allowed a degree of spreading of the shower before it impinged upon a second, significantly thicker ‘R2’ (4.0 radiation-length) tungsten plate, which was followed immediately by the sensor undergoing irradiation. This was closely followed, in turn, by an 8.0 radiation-length tungsten plate. Immediately surrounding the sensor by tungsten radiators that both initiated and absorbed the great majority of the electromagnetic shower ensured that the sensor would be illuminated by a flux of hadrons commensurate with that experienced by a calorimeter sensor close to the

maximum of a tungsten-induced shower. More precise values of the location of the various radiator elements and sensor, for each of the four years of running of T-506, are given in Table 2.

Table 2: Location of the various radiator elements and the sensor under irradiation, for the three successive phases of T-506 running. The R1 radiator had a thickness of $2 X_0$, while the thickness of the R2 radiator was $4 X_0$. The apparent increased geometrical thickness of R2 in Year 1 was due to the presence of a 6mm air gap mid-way through the radiator.

Surface	Year 1	Year 2	Year 3-4
	(2013)	(2014)	(2015-6)
	Location	Location	Location
	(cm)	(cm)	(cm)
R1 Entrance	0.0	0.0	0.0
R1 Exit	0.7	0.7	0.7
R2 Entrance	55.0	45.7	46.6
R2 Exit	57.0	47.1	48.0
Sensor	57.7	47.6	48.5

Although initiating the shower significantly upstream of the sensor promoted a more even illumination of the sensor than would otherwise have been achieved, the half-width of the resulting electron-positron fluence distribution at the sensor plane was less than 0.5 cm. On the other hand, the aperture of the CC apparatus (to be described below) was of order 0.7 cm. Thus, in order to ensure that the radiation dose was well understood over the region of exposure to the CC apparatus source, it was necessary to achieve a uniform illumination over a region of approximately 1 cm^2 . This was done by ‘rastering’ the detector across the beam spot through a range of 1 cm in both dimensions transverse to that of the incident beam. According to Monte Carlo simulation studies, this is expected to generate a region of approximately 1 cm^2 over which the illumination is uniform to within $\pm 20\%$. To account for potential millimeter-level misalignments of the beamline center with the sensor, a ‘targeting factor’ of $(90 \pm 10)\%$ is included in the final dose-rate calculations.

3. Dose Rates

During the 120 Hz operation of the SLAC Linac Coherent Light Source (LCLS), 5-10 Hz of beam was deflected by a pulsed kicker magnet into the End Station transfer line. The LCLS beam was very stable with respect to both current and energy. Electronic pickups and ionization chambers measured the beam current and beam loss through the transfer line aperture, ensuring

that good transfer efficiency could be established and maintained. The transfer efficiency was estimated to be $(95 \pm 5)\%$.

To calculate the dose rate through the sensor, it is necessary to determine the ‘shower conversion factor’ α that provides the mean fluence of minimum-ionizing particles (predominantly electrons and positrons), in particles per cm^2 , per incoming beam electron. This factor is dependent upon the radiator configuration and incident beam energy, as well as the rastering pattern used to provide an even fluence across the sensor (as stated above, the detector was translated continuously across the beam centerline in a 1 cm^2 square pattern).

To estimate α , the Electron-Gamma-Shower (EGS) Monte Carlo program [18] was used to simulate showers through the radiator configuration and into the sensor. The radiator configuration was input to the EGS program, and a mean fluence profile (particles per cm^2 through the sensor as a function of transverse distance from the nominal beam trajectory) was accumulated by simulating the showers of 1000 incident electrons of a given energy. To simulate the rastering process, the center of the simulated profile was then moved across the face of the sensor in 0.5mm steps, and an estimated mean fluence per incident electron as a function of position on the sensor (again, relative to the nominal beam trajectory) was calculated. This resulted in a mean fluence per incident electron that was uniform to within (as stated above) $\pm 20\%$ anywhere inside the boundary of the rastering region. The value of α used for subsequent irradiation dose estimates was taken to be the value found at the intersection of the nominal beam trajectory with the sensor plane. The simulation was repeated for various values of the incident electron energy, producing the values of α shown in Table 3 (Table 4) for the 2013 (2014-16) radiator configuration. For years 2014 through 2016, the spacings of the radiator and sensor were similar enough that a single mean value of α sufficed.

To convert this number to rads per nC of delivered charge, a mean energy loss in silicon of 3.7 MeV/cm was assumed, leading to a fluence-to-rad conversion factor of $160 \text{ rad per nC/cm}^2$. It should be noted that while this dose rate considers only the contribution from electrons and positrons, these two sources dominate the overall energy absorbed by the sensor. In addition, the BeamCal dose-rate spec of 100 Mrad per year considered only the contribution from electrons and positrons.

To confirm the adequacy of the dose-calibration simulation, in 2013 an in-situ measurement of the dose was made using a radiation-sensing field-effect transistor (‘RADFET’) [19] positioned on a daughter board at

Table 3: Shower conversion factor α , giving the mean fluence at the sensor per incident electron, as a function of electron energy, for the 2013 radiator configuration. These values include the effect of rastering over a 1 cm² area surrounding the nominal beam trajectory. Also shown is the number of rads per nC of delivered charge, at the given energy, corresponding to the given value of α .

Beam Energy (GeV)	2013 Shower Conversion Factor α	Dose per nC Delivered Charge (krad)
2	2.1	0.34
4	9.4	1.50
6	16.5	2.64
8	23.5	3.76
10	30.2	4.83
12	36.8	5.89

the expected position of the nominal beam trajectory at the center of the rastering pattern. Beam was delivered in 150 pC pulses of 4.02 GeV electrons; a total of 1160 pulses were directed into the target over a period of four minutes, during which the sensor was rastered quickly through its 1 cm² pattern. The RADFET was then read out, indicating a total accumulated dose of 230 krad, with an uncertainty of roughly 10%. Making use of the dose rate calibration of Table 3, interpolating to the exact incident energy of 4.02 GeV, and taking into account the (95 ± 5)% transfer efficiency of the ESTB beamline, leads to an expected dose of 250 krad, within the ~10% uncertainty of the RADFET measurement.

4. Sensor Irradiation Levels

This proceeding reports on the study of three types of silicon diode sensors. Two pad sensors with p-type and n-type bulk doping (denoted “PF” and “NF”, respectively) were produced from float-zone crystals. A third n-type silicon diode sensor (denoted “LUMI”) was designed for use in the ILC Luminosity Calorimeter. In addition, irradiated bulk (non-diode) GaAs, SiC and industrial sapphire sensors were studied. Once a sensor was irradiated in a 0° – 5° C environment at the ESTB, it was placed in a sub-freezing environment and not irradiated again. Up to four sensors of each type were irradiated and chilled until they could be brought back to the University of California, Santa Cruz campus for the post-irradiation CC and leakage current measurements. In addition, the sub-freezing environment was maintained both during and after the CCE and current measurements, so that controlled annealing studies could be performed. Table 5 displays the dose parameters of the

Table 4: Shower conversion factor α , giving the mean fluence at the sensor per incident electron, as a function of electron energy, for the 2014-16 radiator configuration. These values include the effect of rastering over a 1 cm² area surrounding the nominal beam trajectory. Also shown is the number of rads per nC of delivered charge, at the given energy, corresponding to the given value of α . For 2014 through 2016, the spacings of the radiator and sensor were similar enough that a single mean value of α sufficed.

Beam Energy (GeV)	2014-16 Shower Conversion Factor α	Dose per nC Delivered Charge (krad)
3	4.6	0.73
5	10.0	1.60
7	15.5	2.48
9	21.1	3.38
11	26.7	4.27
13	31.8	5.09
15	37.7	6.03
17	43.0	6.88

irradiated sensors. The (95 ± 5)% transfer line efficiency and the (90 ± 10)% targeting factor have been taken into account in these estimates.

5. Charge Collection Measurement

The SCIPP CC apparatus incorporates a ⁹⁰Sr source that has a secondary β -decay with an end-point energy of 2.28 MeV that illuminate the sensor under study, passing through to a scintillator immediately behind the sensor that is read out by a photomultiplier tube.

For assessing the CCE of pad sensors, a two-stage, single-channel amplifier was constructed from discrete components, based on a design of Fabris, Madden and Yaver [20]. For the first stage, a cascode of two NXP BF862 JFETs is used. The source of the second JFET was connected to the non-inverting input of an LM6171 operational amplifier, chosen for its high slew rate and low input noise contribution. The output of this opamp was then fed back to the input of the first JFET through a 0.05 pF capacitor shunted by a 10 M Ω resistor, completing the negative feedback loop. An external network, including a 32 dB Sonoma Instrument 310 SDI amplifier, was used to further amplify the pulse and shape it to a rise-time of 290 ns.

Upon receiving a trigger from the scintillator, the signal from the amplifier was read out by a Tektronix DPO 4054 digital storage oscilloscope, and the digitized waveforms were written out and stored on the disk of a dedicated data-acquisition computer. After the waveforms were accumulated on the computer, a narrow tem-

Table 5: Dose parameters of the irradiated sensors. A $(95 \pm 5)\%$ transfer line efficiency and a $(90 \pm 10)\%$ targeting factor has been taken into account in final dose estimates.

Sensor	Year	Beam Energy (GeV)	Delivered Charge (μC)	Dose (Mrad)
WSI-P4 (PF)	2015	13.3	50.9	269
N6906 (NF)	2015	14.6	60.0	290
LUMI	2016	(14.5,13.4)	(30.3,37.0)	316
GaAs-09	2014	3.90	21.7	20.8
SiC	2015	13.3	17.2	76.6
Sapphire-04	2016	(14.5,13.4)	(13.1,53.8)	307

poral window was set around the peak of the average excitation pulse from through-going beta particles, and a histogram was made of the resulting pulse-height distribution; a typical distribution is shown in Figure 1. Since not all β particles that trigger the scintillator go through the pad, the distribution shows contributions from both the Landau deposition of the through-going β particles, as well as that of the noise pedestal, allowing for an in-situ subtraction of the mean pedestal.

The amplification system was calibrated by reading out an unirradiated silicon diode sensor of known thickness, and comparing the median charge of the resulting Landau distribution (after subtracting off the mean pedestal) to that expected for an unirradiated sensor of that thickness. The measured gain exhibited only a small dependence on load capacitance. The width of the pedestal distribution then provides a measurement of the readout noise, which was found to be approximately 250 electrons at room temperature.

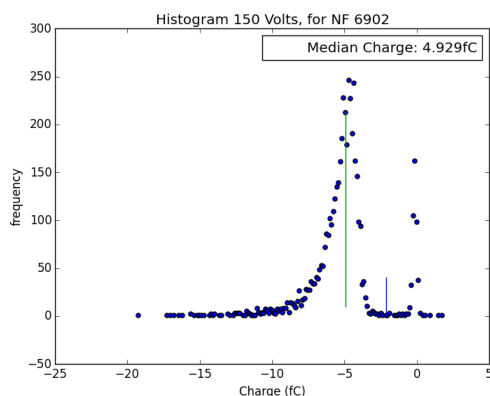


Figure 1: Histogram of pulse height for photomultiplier-triggered data events for the single-channel readout. Both the Landau distribution due to through-going β particles as well as the noise pedestal (for triggers for which the β particle did not traverse the sensor) are seen.

6. Charge Collection and Leakage Current Results

The daughter boards containing the irradiated sensors were designed with connectors that allowed them to be attached to the CC apparatus readout board without handling the sensors. The median CC was measured as a function of bias voltage for each sensor both before and after irradiation, typically after a series of hour-long annealing steps at successively higher temperatures.

6.1. Results for bulk (non-diode) sensors

GaAs has been made use of in sensors designed specifically for use in the BeamCal instrument. The GaAs test structure described in Section 1 was irradiated to a level of 21 Mrad in 2014. Figure 2 exhibits the observed CCE for the GaAs sensor as a function of bias voltage and annealing temperature. Figure 3 shows the CCE as a function of annealing temperature. The sensor exhibited a significant loss in CCE, which worsened after low-temperature annealing but then recovered somewhat after higher-temperature annealing. Figure 4 shows the sensor's pre- and post-irradiation leakage current as a function of temperature, for a bias voltage of $V_B = -600$ V. A significant dependence on sensor temperature is observed, as well as a degradation (increase) after irradiation. This increased leakage current was not observed to improve significantly with annealing.

Industrial sapphire has been proposed as a possible sensor technology for the BeamCal, due to an expectation that it will exhibit radiation tolerance similarly favorable to that of industrial diamond, which is much more costly than industrial sapphire. The intrinsic CCE is low, however, presumably due to a short mean-free path of carriers in the sensor bulk. After exposure to 307 Mrad of electromagnetically-induced radiation, leakage current remained in the nanoamp range over the 1 cm^2 area of the sensor. As illustrated in Figure 5, the median collected charge before irradiation was measured to be only of order 0.3 fC for a detector basis as high as 1000

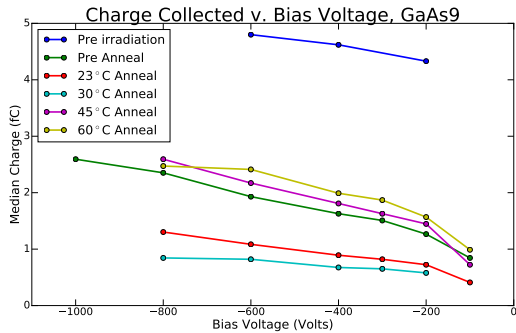


Figure 2: Dependence of the median collected charge from a GaAs sensor upon bias voltage and annealing temperature, after exposure to a dose of 21 Mrad of electromagnetically-induced radiation. Also shown is the median collected charge as a function of bias voltage prior to irradiation.

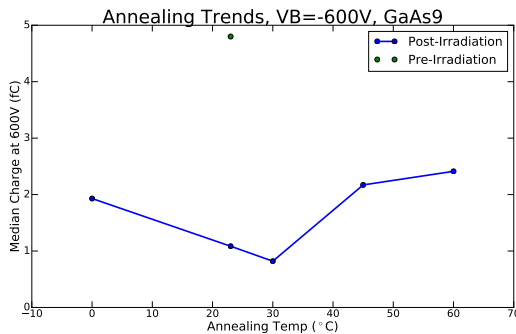


Figure 3: Dependence of the median collected charge from a GaAs sensor upon annealing temperature for a bias of $V_B = -600$ V, before and after exposure to a dose of 21 Mrad of electromagnetically-induced radiation.

V, with a significant drop in CCE observed after irradiation. Figure 6 shows the measure CCE as a function of annealing temperature for biases of ± 1000 V; no improvement is observed over the course of the annealing process.

As illustrated in Figure 7, the sample sensor of 4H silicon carbide with an epitaxial (active) layer thickness of $70 \mu\text{m}$ exhibited charge collection of approximately 0.5 fC before irradiation. After an electromagnetically-induced irradiation of 77 Mrad, substantial loss of CCE was observed at lower bias levels ($V_B \approx 200$ V); however, the CCE was approximately 2/3 of its unirradiated value for $V_B = 1000$ V. As illustrated in Figure 8, little improvement was observed after hour-long annealing episodes at successively higher temperature. Post-irradiation leakage current, measured at approximately

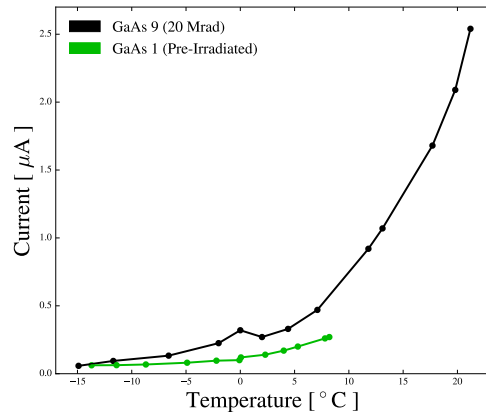


Figure 4: Leakage current vs. temperature for unirradiated and irradiated (21 Mrad) GaAs sensors. The study was done with a bias of $V_B = -600$ V. The irradiated GaAs sensor had been annealed for an hour at a temperature of 75° C.

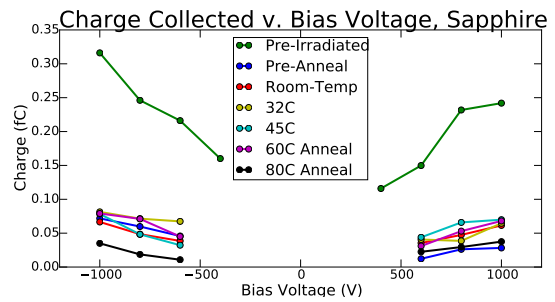


Figure 5: Dependence of the median collected charge from an industrial sapphire sensor upon bias voltage and annealing temperature, after exposure to a dose of 307 Mrad of electromagnetically-induced radiation. Also shown is the median collected charge as a function of bias voltage prior to irradiation.

-15° C, remained at the nanoamp level.

6.2. Results for silicon diode sensors

CCE and leakage current were measured for three types of Si diode sensors after doses of electromagnetically-induced radiation of order 300 Mrad, including both p-bulk (PF) and n-bulk (NF) float zone pad sensors as well as for an n-bulk sensor (LUMI) designed for use in the ILC Luminosity Calorimeter. Figures 9 and 10 exhibit the CCE for the PF sensor before and after a 270 Mrad irradiation, with the post-irradiation CCE exhibited after several successive annealing episodes. Significant CCE loss was observed at lower ($V_B = -200$ V) bias voltages, but for $V_B = -600$ V, the CCE was observed to exceed 80% of its pre-

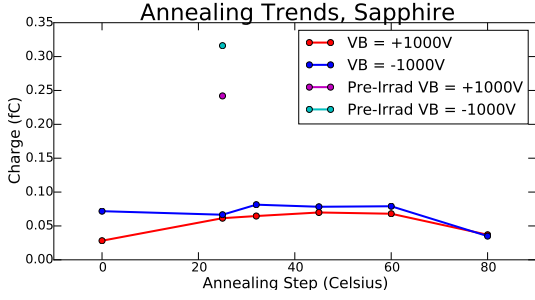


Figure 6: Dependence of the median collected charge from an industrial sapphire sensor upon annealing temperature for biases of ± 1000 V, before and after exposure to a dose of 307 Mrad of electromagnetically-induced radiation.

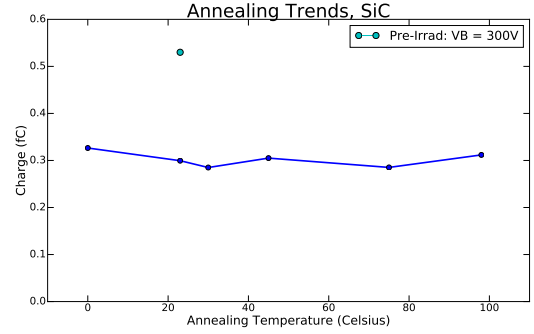


Figure 8: Dependence of the median collected charge from a SiC sensor upon annealing temperature for a bias of $V_B = 600$ V, before and after exposure to a dose of 77 Mrad of electromagnetically-induced radiation.

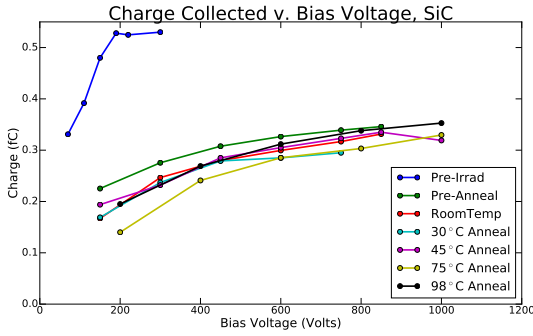


Figure 7: Dependence of the median collected charge from a SiC sensor upon bias voltage and annealing temperature, after exposure to a dose of 77 Mrad of electromagnetically-induced radiation. Also shown is the median collected charge as a function of bias voltage prior to irradiation.

irradiation value after annealing at moderate temperature. Figure 11 shows the PF sensor leakage current observed after irradiation, measured as a function of bias voltage at a temperature of -10° C. Taking into account the 0.025 cm^2 area of the sensor, the current density was measured to be approximately $80 \mu\text{A}/\text{cm}^2$, with little dependence upon annealing temperature. Figure 12 exhibits the post-irradiation leakage current as a function of temperature for a bias voltage of $V_B = -600$ V; the power-law behavior of a doubling of the leakage current for every $5 - 10^\circ$ C increase in temperature is typical for Si diode sensors.

Figures 13 and 14 exhibit the CCE for the NF sensor before and after a 290 Mrad irradiation, with the post-irradiation CCE exhibited after several successive annealing episodes. Again, significant CCE loss was observed at lower ($V_B = 200$ V) bias voltages, while for $V_B = 600$ V, the CCE was observed to approach

60% of its pre-irradiation value after annealing at moderate temperature. The post-irradiation leakage current density was found to be similar in magnitude and temperature dependence to that of the PF sensor discussed above.

Finally, figure 15 exhibits the CCE for the LUMI sensor before and after a 316 Mrad irradiation, with the post-irradiation CCE again exhibited after several successive annealing episodes. The results are qualitatively similar to those for the PF and NF sensors, with significant CCE loss observed for lower bias voltages, but with substantial improvement to the CCE observed for higher bias voltages, particularly after annealing at moderate temperature. Because of the breakdown experienced at bias voltages above several hundred volts (due, again, to the fact that the integrity of the sensor was compromised when it was broken and cleaved, but not expected for an intact sensor), the high-bias CCE behavior could not be explored. Nonetheless, the behavior was observed to be qualitatively consistent with that of the NF sensor discussed above. Given the possibility that significant current was passing across the cleaved edge of the sensor, only an upper bound could be determined for the post-irradiation leakage current for the LUMI sensor. Again, though, this bound suggested qualitative consistency with the NF and PF sensor results.

7. Summary and Conclusions

Using the End Station Test Beam facility at the SLAC National Accelerator Laboratory, we have explored the radiation tolerance of three different types of silicon diode sensors as well as bulk (non-diode) sensors

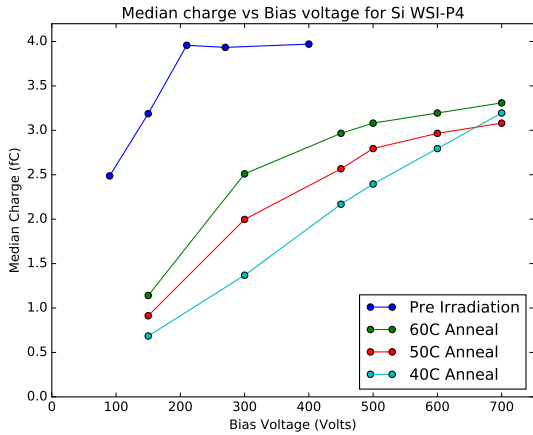


Figure 9: Dependence of the median collected charge from a p-bulk float-zone technology silicon diode sensor upon bias voltage and annealing temperature, after exposure to a dose of 270 Mrad of electromagnetically-induced radiation. Also shown is the median collected charge as a function of bias voltage prior to irradiation.

formed from gallium arsenide, silicon carbide, and industrial sapphire crystals. These sensors were exposed to doses of electromagnetically-induced radiation that varied from 21 Mrad (for the gallium arsenide sensor) to of order 300 Mrad (for the silicon diode and sapphire sensors). At these dose levels, the silicon diode sensors were observed to develop leakage currents of several tens of $\mu\text{A}/\text{cm}^2$ at operating temperatures of -10°C , increasing with temperature with a doubling interval of $5 - 10^\circ\text{C}$. After moderate-temperature annealing, and operating at a reverse bias of 400-600 V, the silicon diode sensors were observed to retain charge-collection efficiency above 50%, with the p-bulk sensor retaining somewhat better charge-collection efficiency than the two n-bulk sensors that were irradiated. The silicon carbide and sapphire sensors, after absorbing doses of 77 and 307 Mrad, respectively, did not develop significant leakage current at an operating temperature of -10°C . Operating at a bias voltage of $V_B = 1000$ V, the silicon carbide sensor retained somewhat over 50% of its unirradiated charge-collection efficiency, while the sapphire sensor retained only about 20% of its unirradiated charge-collection efficiency. Neither sensors showed improvement with annealing. Finally, after moderate temperature annealing, the gallium arsenide sensor retained approximately 50% of its original charge-collection efficiency after a 21 Mrad dose. Somewhat unexpectedly, the sensor was observed to develop a leakage current of approximately $1 \mu\text{A}/\text{cm}^2$ at an op-

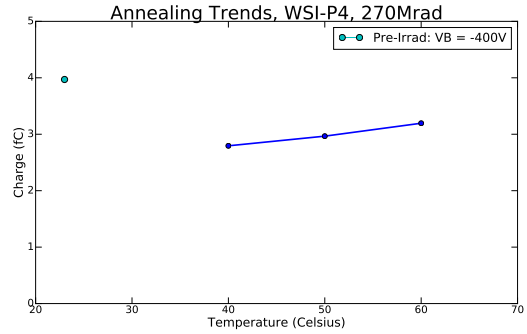


Figure 10: Dependence of the median collected charge from a p-bulk, float-zone technology silicon diode sensor as a function of annealing temperature for a bias of $V_B = -600$ V, before and after exposure to a dose of 270 Mrad of electromagnetically-induced radiation.

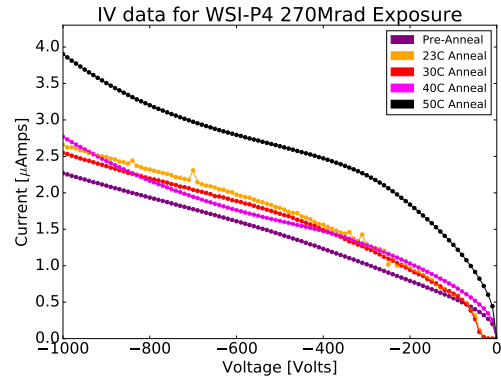


Figure 11: Dependence of the leakage current through a p-bulk float-zone technology silicon diode sensor upon bias voltage and annealing temperature, after exposure to a dose of 270 Mrad of electromagnetically-induced radiation.

erating temperature of -10°C , with a fractional rate of increase with temperature similar to that of the silicon diode sensors. These gallium arsenide results await confirmation with a sensor that has been irradiated to 100 Mrad but has not yet been characterized.

8. Acknowledgments

We are grateful to Leszek Zawiejski, INP, Krakow for supplying us with the tungsten plates needed to form our radiator, Georgy Shelkov, JINR, Dubna for supplying us with GaAs sensors for irradiation studies, Bohumir Zatkó, Slovak Academy of Sciences, for supplying us with the SiC sensor, and Sergej Schuwalow, DESY Zeuthen, for supplying us with the industrial sapphire sensor. We

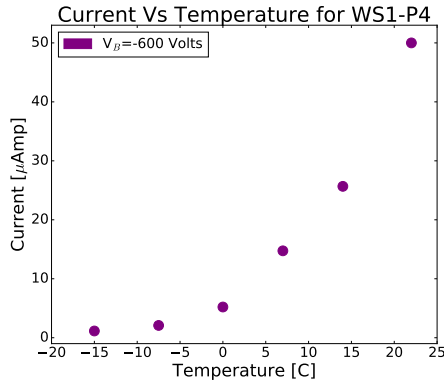


Figure 12: Dependence of the leakage current through a p-bulk float-zone technology silicon diode sensor upon temperature after exposure to a dose of 270 Mrad of electromagnetically-induced radiation. The sensor was biased to $V_B = -600$ V.

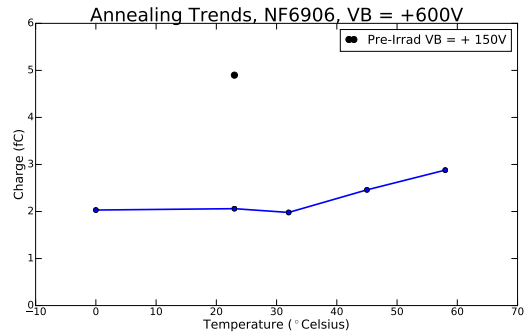


Figure 14: Dependence of the median collected charge from an n-bulk, float-zone technology silicon diode sensor as a function of annealing temperature for a bias of 600 V, before and after exposure to a dose of 290 Mrad of electromagnetically-induced radiation.

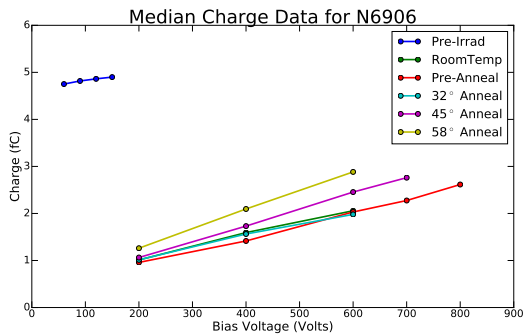


Figure 13: Dependence of the median collected charge from an n-bulk float-zone technology silicon diode sensor upon bias voltage and annealing temperature, after exposure to a dose of 290 Mrad of electromagnetically-induced radiation. Also shown is the median collected charge as a function of bias voltage prior to irradiation.

would also like to express our gratitude to the SLAC Laboratory, and particularly the End Station Test Beam delivery and support personnel, who made the run possible and successful. Finally, we would like to thank our SCIPP colleague Hartmut Sadrozinski for the numerous helpful discussions and guidance he provided us.

9. Role of the Funding Source

The work described in this article was supported by the United States Department of Energy, DOE contract DE-AC02-7600515 (SLAC) and grant DE-FG02-04ER41286 (UCSC/SCIPP). The funding agency played no role in the design, execution, interpretation, or documentation of the work described herein.

References

- [1] ILD Concept Group, *International Large Detector DBD*, <http://www.linearcollider.org/ILC/physics-detectors/Detectors/Detailed-Baseline-Design>, Chapter 4 (2012).
- [2] SID Collaboration, *SiD Detailed Baseline Design*, <http://www.linearcollider.org/ILC/physics-detectors/Detectors/Detailed-Baseline-Design>, Chapter 5 (2013).
- [3] J.R. Carter and R.G. Downing, 'Charged Particle Radiation Damage in Semiconductors: Effect of Low Energy Protons and High Energy Electrons on Silicon', Interim Technical Final Report, TRW Apce Technology Laboratories, May 1965.
- [4] T. Noguchi and M. Uesugi, 'Electron Energy Dependence of Relative Damage Coefficients of Silicon Solar Cells for Space Use', Technical Design of the International PVSEC-5, Kyoto, Japan (1990).
- [5] Geoffrey P. Summers *et al.*, 'Damage Correlations in Semiconductors Exposed to Gamma, Electron, and Proton Radiations', IEEE Transactions on Nuclear Science 40, 1372 (1993).
- [6] J.M. Rafi *et al.*, 'Degradation of High-Resistivity Float Zone and Magnetic Czochralski n-type Silicon Detectors Subjected to 2-MeV Electron Irradiation', NIM A 604, 258 (2009).
- [7] S. Dittongo *et al.*, 'Radiation Hardness of Different Silicon Materials after High-Energy Electron Irradiation', NIM A 530, 110 (2004).
- [8] S. Dittongo *et al.*, 'Studies of Bulk Damage Induced in Different Silicon Materials by 900 MeV Electron Irradiation', NIM A 546, 300 (2005).
- [9] G. Casse *et al.*, 'First Results on Charge Collection Efficiency of Heavily Irradiated Microstrip Sensors Fabricated on Oxygenated p-type Silicon', NIM A 518, 340 (2004).
- [10] G. Casse, 'Radiation Hardness of p-type Silicon Detectors', NIM A 612, 464 (2010).
- [11] Y. Unno *et al.*, *Development of n-on-p silicon sensors for very high radiation environments*, NIM A 636, S24 (2011).
- [12] T. Ohsugi *et al.*, *Design and properties of the GLAST flight silicon micro-strip sensors*, NIM A 541, 29 (2005).
- [13] W. Wierba *et al.*, 'Silicon Sensors for LumiCal Status Report', EUDET-Memo-2008-12 (2012).
- [14] K. Afanaciev *et al.*, 'Investigation of the radiation hardness of GaAs sensors in an electron beam', JINST 7, P11022 (2012).
- [15] B. Zatko *et al.*, 'Radiation detector based on 4H-SiC used for Thermal Neutron Detection', JINST 11, C11022 (2016).

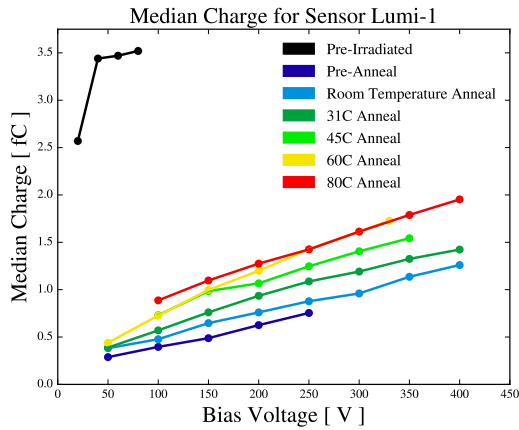


Figure 15: Dependence of the median collected charge from a fragment of an n-bulk silicon diode sensor designed for use with the ILC Luminosity Calorimeter, as function of bias voltage and annealing temperature, after exposure to a dose of 316 Mrad of electromagnetically-induced radiation. Also shown is the median collected charge as a function of bias voltage prior to irradiation.

[16] R. Band *et al.*, 'Initial results of a silicon sensor irradiation study for ILC extreme forward calorimetry', NIM A 765, 41-16 (2014).

[17] G. Courcoubetis *et al.*, 'Updated Results of a Solid-State Sensor Irradiation Study for ILC Extreme Forward Calorimetry', Proceedings of the 2015 International Workshop on Future Linear Colliders (LCWS15), Whistler, B.C., Canada, 02-06 November 2015, arXiv:1602.08552 [physics.ins-det].

[18] The Electron Gamma Shower (EGS) Monte Carlo Program, <http://rcwww.kek.jp/research/egs/>.

[19] The specific device used was the REM Oxford Ltd. corporation's REM TOT601B device, <http://www.radfet.com/index.html>.

[20] L. Fabris, N. W. Madden and H. Yaver, 'A fast, compact solution for low noise charge preamplifiers', NIM A 424, 545-551 (1999).